Met. Mater. Int., Vol. 23, No. 4 (2017), pp. 764~769
doi: 10.1007/s12540-017-6732-7

Numerical Simulation of Hydrogen Desorption From High-Density Metal Hydride Hydrogen Storage Vessels

Sang-Kun O[1,*], Kyung-Woo Yi[1,*], and Sung-Wook Cho[2]

[1]Department of Materials Science and Engineering, Seoul National University, Seoul 08826, Republic of Korea
[2]Resources Utilization Research Center, Korea Institute of Geoscience & Mineral Resources, Daejeon 34132, Republic of Korea

(received date: 14 October 2016 / accepted date: 15 December 2016)

Metal hydride (MH) alloys are a promising type of material in hydrogen storage applications, allowing for low-pressure, high-density storage. However, while many studies are being performed on enhancing the hydrogen storage properties of such alloys, there has been little research on large-scale storage vessels which make use of the alloys. In particular, large-scale, high-density storage devices must make allowances for the temperature variations caused by the heat of reaction between hydrogen and MH alloys, which may impact the storage characteristics. In this study, we propose a numerical model for the design and evaluation of hydrogen storage devices using MH alloys. Hydrogen desorption reaction behavior for an alloy is observed in terms of temperature and reaction rate. This behavioral correlation is used as the basis for a comprehensive simulation model of the alloy system. Calculated results are found to be in good agreement with experimentally measured data, indicating that the model may be applied to multiple system geometries, scales, and alloy compositions.

Keywords: hydrogen absorbing materials, hydrogen, metal hydride, thermal conductivity, computer simulation

1. INTRODUCTION

Hydrogen storage is a major obstacle in the development of a viable, efficient hydrogen economy [1]. Existing storage technologies, such as high pressure gas as liquid-state storage, are limited by issues such as low volumetric storage density, instability and cost. As an alternative, numerous previous studies have demonstrated that certain metal alloys may be used in hydrogen storage applications due to their ability to absorb and release hydrogen, with no significant degradation of their structure over the course of multiple cycles. Moreover, metal hydride hydrogen storage offers potential benefits such as high volumetric density and stable, low pressure utilization [1]. Examples of such alloys include the TiCrV alloy [2, 3] and TiCrV-Fe alloy [4]. These alloys have demonstrated reasonably high reversible storage capacities and resiliency for multiple cycles. Additionally, studies have also been performed to investigate processes to facilitate hydriding and dehydriding such materials through measures such as mechanical grinding and the use of additives [5-7].

However, despite the active studies being performed on materials for metal hydride hydrogen storage, only a comparatively limited amount of research has been done on the bulk behavior or storage device designs for such materials in large-scale applications.

Moreover, due to constraints arising from factors such as high cost and practicality, production of large amounts of alloys and direct experimentation on multiple devices which make use of such alloys are prohibitively difficult unless a justifiably effective design is pre-determined. Thus, insightful studies regarding the impact of various functioning variables on device efficiency may focus primarily on a single design [9].

A convenient and reliable alternative to such direct experimentation is to predict the characteristics of various designs through numerical simulation. A number of such studies have been reported in the literature [10-13]. Many studies, however, are not performed in tandem with direct analysis of real MH alloy samples, but based on pre-existing systems as reported in the literature. Another limitation is that many reported results derived from numerical analysis are aimed more at evaluating a proposed system, rather than offering a new design direction.

In this study, we perform numerical simulations for multiple tank geometries, in tandem with actual pilot scale experimentation, in order to overcome these limitations. The numerical model to comprehensively simulate hydrogen desorption behavior in MH tanks employs various parameters such as heat of hydride reaction and thermal properties taken from experiments using a TiCrV-Fe alloy. The accuracy of the numerical simulations are verified through comparison with data mea-

*Corresponding authors: osang01@snu.ac.kr, yikw@snu.ac.kr

sured from a pilot system. The predictive and analytical capabilities of the model may be expected to be applied to multiple system geometries, scales, alloy compositions and applications.

2. EXPERIMENTAL PROCEDURE

2.1. Development of numerical model

As pointed out in earlier studies [16], metal hydride materials will generally reach a uniform particle size following several cycles of hydrogenation and dehydrogenation, and therefore the powder bed is assumed to be a homogeneous volume of uniform conductivity, density and porosity. The major parameters considered for numerical simulation in this study are temperature variations caused by the reaction heat, and reaction rate.

The reaction heat of hydrogen absorption or desorption will result in a change of the MH alloy's temperature, which in turn will influence the reaction rate. The heat is transported through two major steps: it is transferred within the bulk of the device by thermal conduction, and introduced to the system or released to the surrounding atmosphere by convective heat transfer. The effective thermal conductivity, i.e. the rate at which heat can be conducted into or out of the device, is of particular importance in determining the efficiency of a device [1,8,9,14], especially given the unpredictable conductivity of porous materials [14,15]. The thermal conductivity value of alloy powder in the present study is taken from measurement of a sample. The steps of heat generation and absorption, conduction and convection are all considered in numerical calculations. Heat transfer is calculated through an energy conservation equation. The CFD-ACE general purpose commercial numerical analysis software package employed in the present study makes use of the total enthalpy equation.

The magnitude of the reaction heat and its correlation with the system temperature and resulting reaction rate are at the core of the model presented in this study. Initial values for concentration, temperature and reaction rate are given for the system. For each time step, the concentration value will decrease depending on the reaction rate. The amount of reacted hydrogen will also determine the reaction heat, which in turn determines the change in temperature. The new temperature and hydrogen concentration then become the basis for the new reaction rate.

Hence, the reaction rate may be defined as a function of temperature and concentration, or

$$R = f(T,C) \tag{1}$$

where R is the reaction rate, T is the temperature, and C is the hydrogen concentration.

While this relationship may be determined experimentally for any MH alloy, in some cases the variable C has only a negligible effect on the reaction rate. In such cases, in the interest of calculation efficiency and simplicity, we may omit C from the relationship and define the reaction rate as

$$R = f(T) \tag{2}$$

This correlation between temperature, concentration and reaction rate is taken from measurements on an experimental system, which will be outlined in the subsequent section.

However, this basic algorithm requires that no limitation is placed on the reaction of hydrogen and MH alloy, i.e. any reaction which is allowed by the temperature condition will indeed take place. But in practice, it is far more likely that a user-designated reaction rate will be imposed on the system depending on the amount of hydrogen gas which is required for the application over time.

To account for this, we implement a variable 'k' which we term as the 'rate factor.' Additionally, to account for local variations, we distinguish between R, the reaction rate for any given cell in a model system, and Q, the total flow rate which results from the system as a whole.

The amount of total flow which temperature and concentration conditions allow is called Q_P, the total flow rate (potential), and defined as

$$Q_P = \frac{\sum f(T_i, C_i) \times V_i}{\sum V_i} \tag{3}$$

where T_i, C_i and V_i respectively represent the temperature, concentration and volume of each cell with index i.

The actual total flow, which is limited by a user designated amount, is then given as Q_R: Total flow rate (real) and defined as

$$Q_R = k \times Q_P \tag{4}$$

thus giving us the definition for the rate factor, k, as

$$k = Q_R / Q_P \tag{5}$$

Hence, if $k < 1$, less gas reaction occurs than the temperature

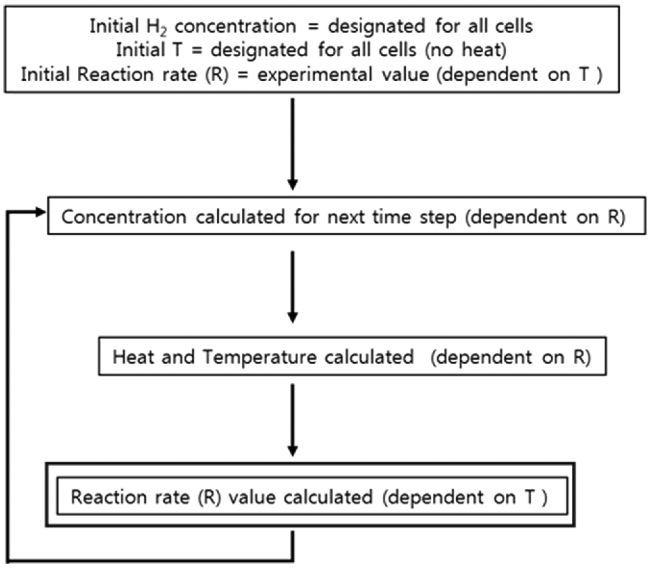

Fig. 1. Schematic representation of comprehensive numerical algorithm.

and concentration allow. If $k \geq 1$, the reaction rate allowed by temperature and concentration is less than the user designated limited, so that the entire potential reaction rate does indeed occur. Therefore, it stands to reason that k cannot ever exceed 1.

The model is calculated according to a comprehensive algorithm as represented schematically in Fig. 1. The calculation is carried out in the following order:

1. Initial values are given for T, C, R_P (as defined by $R = f(T,C)$) and Q_R
2. For the entire system,
   a. $Q_p = \dfrac{\sum f(T_i, C_i) \times V_i}{\sum V_i}$
   b. $k = Q_r / Q_p$
      if $k < 1$, $k = k$
      if $k \geq 1$, $k = 1$
   c. $Q_R = k \times Q_P$
3. For each computational cell,
   a. $R_R = k \times R_P$
   b. C diminishes according to R_R
   c. Reaction heat is determined by $R_R \rightarrow$ calculate T
   d. $R_P = f(T,C)$ from new T and C values
4. Steps 2-3 are repeated for each time step of the simulation

This algorithm allows us to calculate the transient potential reaction rate, the real reaction rate, temperature and hydrogen concentration for any locality in a system over a period of time.

In the present study, we use CFD-ACE, a commercial software package for numerical analysis. We employ our own independently developed subroutine in order to reflect the changes in concentration, heat and reaction rate as described in the model above.

2.2. Experiments on metal hydride characteristics

The specifics of Eqs. (1) and (2), that is, the correlation between temperature, concentration and reaction rate, must be taken from measurements on an experimental system using the MH alloy in question.

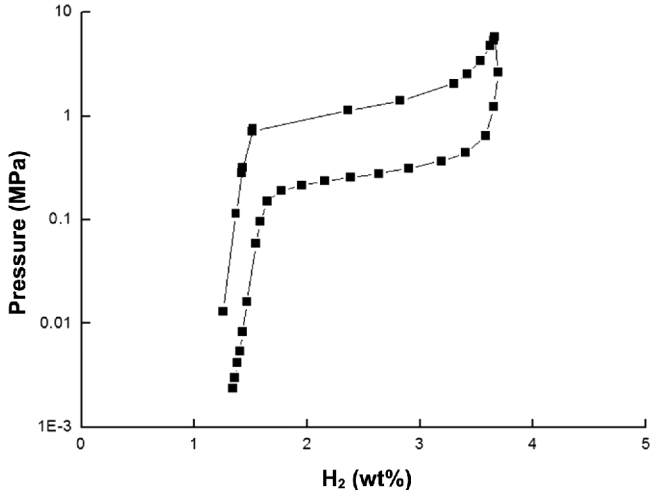

Fig. 2. PCT characteristics of $Ti_{0.32}Cr_{0.35}V_{0.25}$-$Fe_{0.08}$ alloy at 293 K.

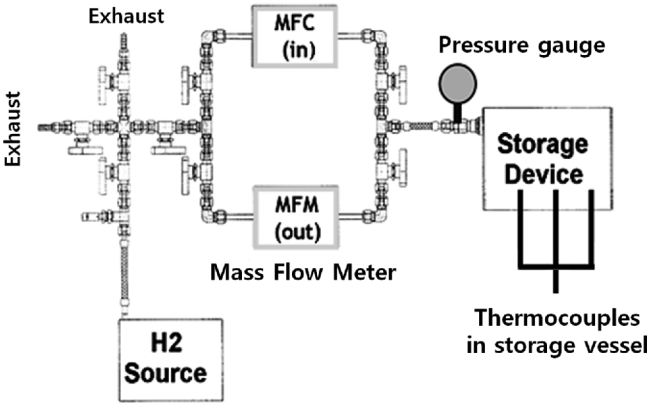

Fig. 3. Experimentation system with a simple hydrogen storage device.

In the present study, the simulations are based on direct experimental measurements of $Ti_{0.32}Cr_{0.35}V_{0.25}$-$Fe_{0.08}$ alloy. The PCT characteristics of the alloy at 293 K are given in Fig. 2. The alloy demonstrates a relatively high reversible storage capacity within a reasonable pressure range. Reaction heat for the alloy considered in this study was measured in samples to be 42 kJ for each mole of reacted hydrogen gas.

In order to obtain bulk-scale data of the TiCrV-Fe alloy used in the present study, we built an experimentation system with a simple hydrogen storage device. The system, as illustrated in Fig. 3, consists of a MH tank filled with 1 kg of TiCrV-Fe alloy, a mass flow meter, and a mass flow controller. Multiple strategically placed thermocouples make it possible to obtain both localized and average temperature readings from within the MH alloy tank during reaction. Gas flow rates for absorption and desorption are measured through the mass flow controller and mass flow meter, respectively.

2.3. Verification of model through comparison with experiments

To ensure that the numerical model is accurate and reasonable, we performed direct experimentation on two test tanks under various conditions. As illustrated in Fig. 4(a), the stainless steel tanks are in the shape of a cylinder, with copper fins fitted inside to allow for better heat conduction. The inner interior dimensions of the tanks measure 200 mm high with a radius of 140mm. Each of the tanks is filled with 5 kg of TiCrV-Fe alloy. The exterior of the tanks is fitted with heaters, which allows for constant regulation of the surface temperature. Reaction rate and resulting gas flow rate are controlled (i.e. limited) through a mass flow controller. A 3D numerical model grid of the system with 21,920 computational cells was created as shown in Fig. 4(b), with the copper fins and interior of the steel liner shown in dark lines, and the algorithm described above was applied for the various experimentation conditions to compare measured and simulated results.

Experiments on the test tanks illustrated in Fig. 4 were per-

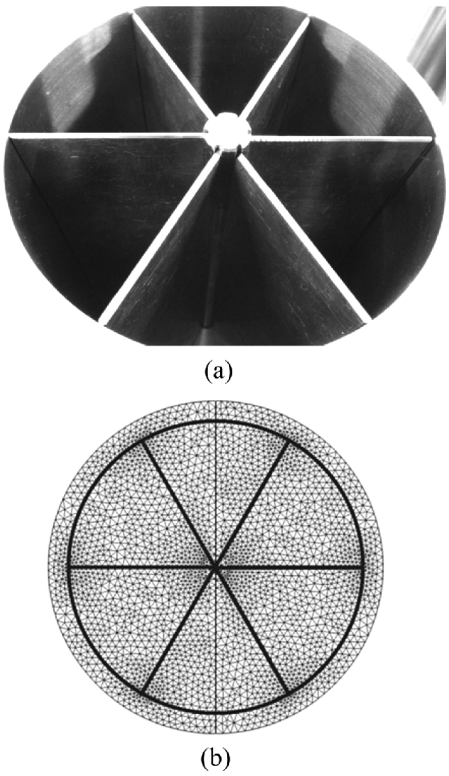

Fig. 4. Structure of test tank (a) and its numerical model grid (b).

formed with a set flow limit of 5 L/min for each tank, for a total of 10 L/min. The external temperature was kept constant by use of an external heater. Hydrogen gas desorption and release was allowed up to the limited flow rate starting from an initial charge pressure of 35 atm and pre-heating to make the overall temperature within the tank uniform.

3. RESULTS AND DISCUSSION

3.1. Measured characteristics of MH alloy

The experimental system allows for measurement of average temperature, reaction rate, and hydrogen concentration within the MH alloy, each over time. Therefore, the value of each of the three variables at any time constitute coordinates which, when taken together, can be generalized with a fitting equation. This fitting equation of the data yields the reaction rate defined as a function of temperature and concentration, or

$$R = f(T,C) \quad (1)$$

In the case of the TiCrV alloy used in the present study, the variable C was found to have only a negligible effect on the reaction rate. This is likely due to the low system pressure and relatively constant equilibrium pressure during desorption, as shown in Fig. 2. As a result, it is reasonable to omit C from the relationship and define the reaction rate as

$$R = f(T) \quad (2)$$

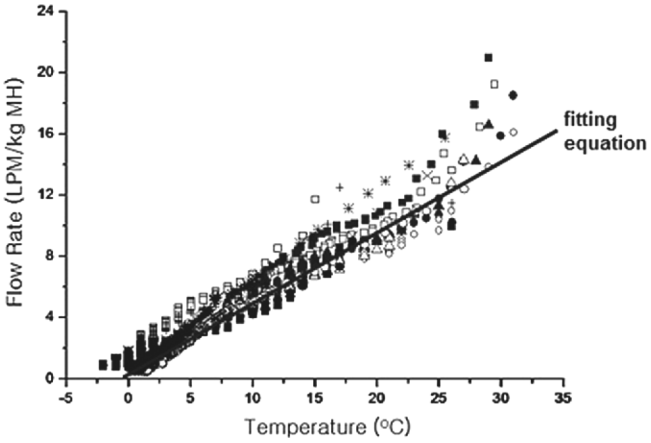

Fig. 5. R = f(T) where R is reaction rate and T is temperature.

which is shown graphically in Fig. 5. By finding a fitting equation for the multiple experimental trials as shown in Fig. 5, we find that the relationship defined by Eq. (2) may be given as

$$R = (T/540)\ (\%/sec) \quad (6)$$

for the TiCrV-Fe alloy used in this study, specifically. This equation is then applied to the numerical model as detailed in Section 2.

3.2. Verification of model through comparison with experiments

Figure 6 shows the measured vs. calculated reaction rate over time for trials with flow limited to 5 slpm from each tank, for a total of 10 slpm, with maintained external temperature of 30 °C and 40 °C, respectively. In each case, we can observe that initially, the flow rate is maintained at the limited value. However, as the endothermic reaction gradually lowers the overall system temperature, eventually the system reaches a point at which the alloy temperature results in a lower reaction rate which can no longer support the designated flow rate, and the flow rate drops after that point. For both of the external heating conditions, this trend is expected, and shown to demonstrate good agreement between measured and calculated results.

However, for both cases it is clear that the measured results indicate a longer period during which the designated flow rate is maintained by the system, before the flow rate diminishes to below the designated value. In both cases, that difference in time during which the flow rate is maintained between measured and calculated results is found to be approximately 300 sec, or 5 minutes. That this time difference is nearly identical despite different experimental conditions indicates that the value arises from a factor which the two tanks share in common.

We have found that given a porosity of approximately 0.49 for the MH alloy powder and the dimensions of the tank, roughly 1.4 L in combined volume exists within the tanks which

are not filled by the powder itself; in other words, that volume is filled by free gas which has not reacted with or from the powder. Given the initial hydrogen charging process, this results in approximately 50 L of free gas which is released from the tank prior to reaction and release from the MH alloy, which fits accurately with the 5 minutes of gas flow at 10 LPM, the gap between the calculated and experimental results.

In short, the discrepancy in the calculated vs. experimental results was a result of a failure to take into account the free gas which is released from the tanks regardless of reaction from the MH alloy. The amount of this initial release of free gas prior to MH alloy reaction will depend on the dimensions of the tank, and the temperature and pressure conditions of the initial charge.

Taking into account this additional factor, we add the expected period of gas release at the designated flow rate to the initial point of the simulation, which gives us a much better agreement between calculated and measured results. Figure 6(b) shows results of measurement and calculation for gas release with the initial, non-reactive gas release from the early stages of the trials taken into account. In these results, we find that the calculated and measured values are indeed in excellent agreement.

Given that the reaction rate is taken to be dependent on the temperature, we can also examine the behavior of the tank in terms of the temperature variation, both locally and as a whole. Figure 7(a) shows the change in the average temperature of the MH region within the tank over time, for a trial as detailed in Fig. 6 with flow limited to 5 slpm from each tank, for a total of 10 slpm, and a maintained external temperature of 30 °C. The average temperature value will determine the overall reaction and flow rates, as defined by Eq. 2. With progression of time, the endothermic reaction lowers the overall temperature of the system, until it reaches a critical temperature at which the reaction rate made possible by the tempera-

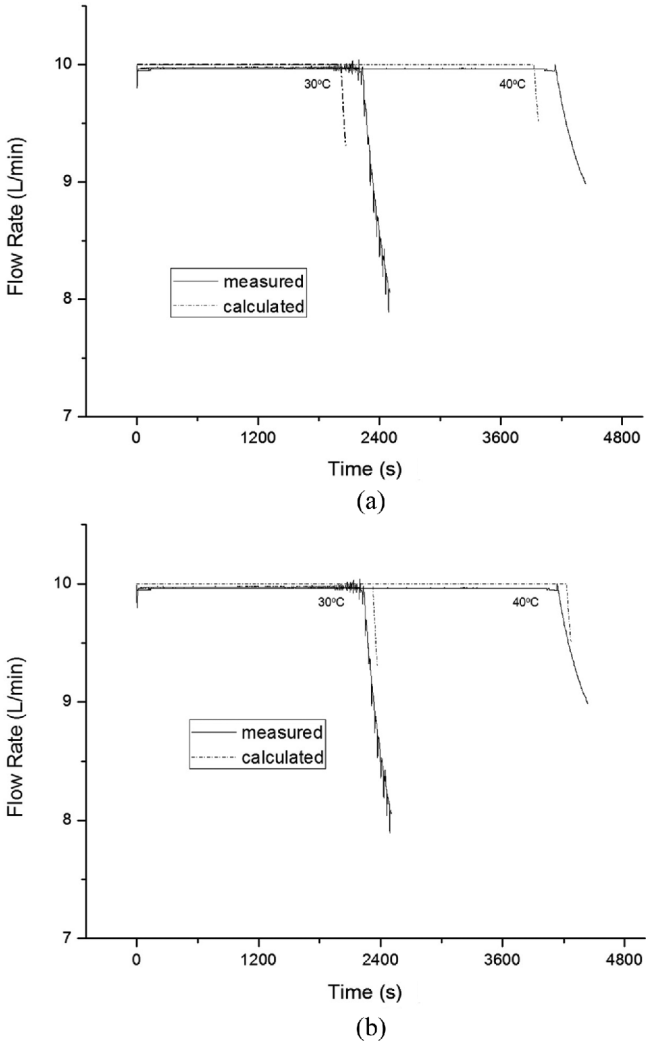

Fig. 6. Measured vs. calculated reaction rate over time for two tanks limited at 5 LPM each, with maintained external temperature of 30 °C and 40 °C, given for calculation of immediate gas reaction (a) and for calculations reflecting initial free gas release (b).

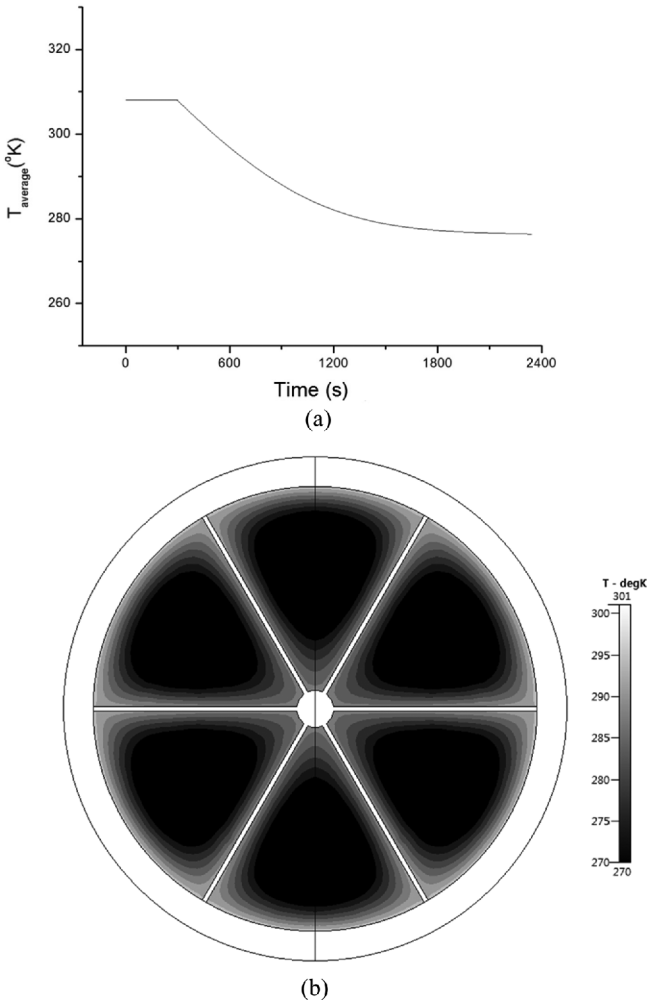

Fig. 7. Change in the average temperature of the MH region within the tank over time (a) and cross-sectional view of temperature distribution of MH region (b).

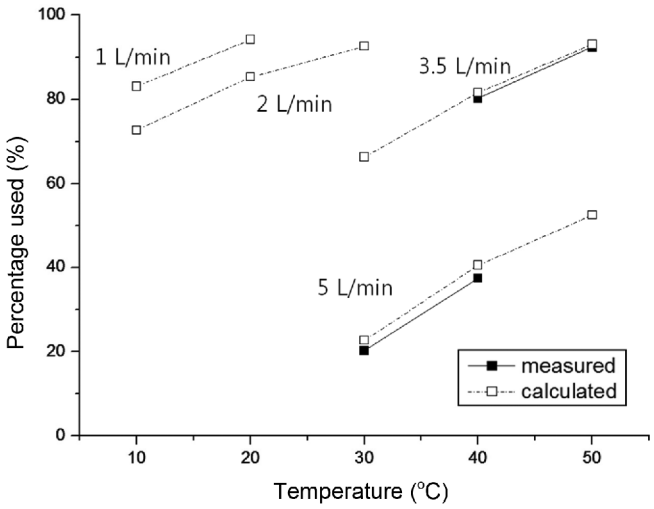

Fig. 8. Measured and calculated values for the percentage of the total hydrogen capacity of the MH alloy in the experimental tank which is released at the designated flow rate, for various external temperature or designated flow rate conditions.

ture is insufficient to produce the designated flow rate limit.

While the average temperature value will determine the overall reaction and flow rates, it is also worth noting that there will be local variations of temperature depending on the location within the tank geometry. The present model allows for time-dependent calculation of these local temperature differences. An example of this is given in Fig. 7(b), which shows a cross section of the tank with temperature given for the MH region at the point in time at which the temperature can no longer support the designated flow rate. It is worth noting that temperatures higher than the average can be found near the tank wall, and near the high-conductivity interior fins, as these areas allow heat to be transferred more readily from the surface heater to the MH region. In contrast, the regions of MH furthest from the tank wall and high-conductivity fins are seen to have relatively lower temperatures. From this observation, we can conclude that the overall variation of local temperature in an MH bed will depend on the tank geometry, and consequently the tank geometry plays a major role in the reaction kinetics of an MH system. This ability of the present model to interpret local temperature variation over time is expected to be of great use in future designs and evaluations of different tank systems.

Given the reliability of the model as demonstrated through comparison with experimental results, the model can be used in a variety of ways to predict tank behavior for various operation conditions, or to evaluate a tank design. Figure 8 shows measured and calculated values for the percentage of the total hydrogen capacity of the MH alloy in the experimental tank which is released at the designated flow rate, depending on the external temperature and designated flow rate. For flow rates of both 3.5 LPM and 5.0 LPM, and at various temperatures, we see an excellent agreement between measured and calculated values. Building on the accuracy of the model, we can then predict the values for various other external temperature or designated flow rate conditions with a high degree of confidence.

4. CONCLUSION

In this study, we propose a numerical model for the design and evaluation of hydrogen storage devices using MH alloys. Hydrogen desorption behavior for an alloy was observed in terms of temperature and reaction rates. This behavioral correlation was then used as the basis for a comprehensive simulation model the alloy system, which allows analysis of system temperature and reaction rate changes over time. Comparison between results from direct experimentation on a test tank and results calculated from a numerical model of said tank show excellent agreement. As such, the model may be expected to be applied to multiple system geometries, scales, and alloy compositions.

REFERENCES

1. G. Sandrock, *J. Alloy. Compd.* **293-295**, 877 (1999).
2. H. C. Lin, K. M. Lin, K. C. Wu, H. H. Hsiung, and H. K. Tsai, *Int. J. Hydrogen Energ.* **32**, 4966 (2007).
3. S.-W. Cho, G. Shim, G.-S. Choi, C.-N. Park, J.-H. Yoo, and J. Choi, *J. Alloy. Compd.* **430**, 136 (2007).
4. J.-H. Yoo, G. Shim, S.-W. Cho, C.-N. Park, *Int. J. Hydrogen Energ.* **32**, 2977 (2007).
5. M. Y. Song, Y. J. Kwak, S. H. Lee, and H. R. Park, *Met. Mater. Int*. **21**, 207 (2015).
6. S. H. Lee, H. R. Park, and M. Y. Song, *Korean J. Met. Mater.* **53**, 133 (2015).
7. S. H. Lee, Y. J. Kwak, H. R. Park, and M. Y. Song, *Korean J. Met. Mater*. **53**, 187 (2015).
8. J. Zhang, T. Fisher, P. V. Ramachandran, J. P. Gore, and I. Mudawar, *J. Heat Transf.* **127**, 1391 (2005).
9. P. Muthukumar, M. P. Maiya, and S. S. Murthy, *Int. J. Hydrogen Energ.* **30**, 1569 (2005).
10. M. Gambini, M. Manno, and M. Vellini, *Int. J. Hydrogen Energ.* **33**, 6178 (2008).
11. B. D. MacDonald and A. M. Rowe, *Int. J. Hydrogen Energ.* **31**, 1721 (2006).
12. B. D. MacDonald and A. M. Rowe, *J. Power Sources* **161**, 346 (2006).
13. T. Oi, K. Maki, and Y. Sakaki, *J. Power Sources* **125**, 52 (2004).
14. M. Nagel, Y. Komazaki, and S. Suda, *J. Alloy. Compd.* **120**, 35 (1986).
15. A. Kurt and H. Ates, *Mater. Design* **28**, 230 (2007).
16. G. Mohan, M. Prakash Maiia, S. Srinivasa Murthy, *Int. J. Hydrogen Energ.* **32**, 4978 (2007).